International Journal of Concrete Structures and Materials
Vol.10, No.4, pp.499–511, December 2016
DOI 10.1007/s40069-016-0172-5
ISSN 1976-0485 / eISSN 2234-1315

An Analytical Model for FRP Debonding in Strengthened RC Beams under Monotonic and Cyclic Loads

Reza Saeidi Moein, and Abbas Ali Tasnimi*

(Received December 1, 2015, Accepted September 28, 2016, Published online November 18, 2016)

Abstract: Reinforced concrete (RC) beams strengthened by externally bonded reinforcement often fail by debonding. This paper presents an experimental and analytical study aimed at better understanding and modeling the fiber reinforced polymer (FRP) debonding failures in strengthened RC beams under monotonic and cyclic loads. In order to investigate the flexural behavior and failure modes of FRP-strengthened beams under monotonic and cyclic loadings, an experimental program was carried out. An analytical study based on the energy balance of the system was also performed. It considers the dominant mechanisms of energy dissipation during debonding and predicts the failure load of the strengthened beams. Validation of the model was carried out using test data obtained from the own experimental investigation.

Keywords: analytical model, CFRP laminate, debonding, experimental study, RC beam, strengthening.

List of symbols

c	Neutral axis depth
c_1	Neutral axis depth, before debonding failure
c_2	Neutral axis depth, after debonding failure
d	Effective depth of beam section
$d_{a,max}$	Maximum aggregate size
$f_c^{'}$	Compressive strength of concrete
f_{ct}	Tensile strength of concrete
f_y	Yield strength of steel rebar
l_a	Bond length at interface between flexural FRP laminate and end anchorage
l_c	Length of constant moment region
l_f	Bonded length of flexural FRP laminate
l_s	Shear span
w/c	Water/cement ratio of concrete
w_a	Width of wrapped FRP sheet (end anchorage)
w_c	Width of concrete member
w_f	Bonded width of flexural FRP laminate
A_f	Interfacial bond area
A_s	Total cross-sectional area of steel rebar
$\mathbf{D}$	Irreversible energy dissipation of the system
D_{FRP}^{d}	Energy dissipation due to debonding of FRP laminate
D_{st}^{y}	Energy dissipation due to yielding of steel rebar
E	Elastic modulus of concrete
G_f	Bond fracture energy
$G_{C,I}$	Mode-I fracture energy of concrete
$G_{C,II}$	Mode-II fracture energy of concrete
$G_C(\theta)$	Mixed-mode fracture energy of concrete
$G_{F,I}$	Mode-I fracture energy of interface
$G_{F,II}$	Mode-II fracture energy of interface
$G_F(\theta)$	Mixed-mode fracture energy of interface
I_c	Moment of inertia of transformed cross-section of control beam in cracked condition
I_s	Moment of inertia of transformed cross-section of strengthened beam in cracked condition
k_b	A geometric factor that considers the influence of the laminate width relative to the width of the concrete member
K_c	Stiffness of control beam tested in four-point bending
K_s	Stiffness of strengthened beam tested in four-point bending
L	Span length of the beam
P_{dc}	Load of control beam corresponding to the deflection of Δ_{dc}
P_{ds}	Load of strengthened beam at the debonding failure deflection of Δ_{ds}
P_{yc}	Load of control beam at rebar yielding
$P_{fs}^{\delta_d}$	Failure load of strengthened beam at the debonding displacement of δ_d
$P_{fu}^{\delta_d}$	Load of control beam corresponding to the displacement of δ_d
$\mathbf{T}$	Surface tractions acting at boundary of the system
$\mathbf{W}^{ext}$	Externally supplied work of the system
$\mathbf{W}$	Global free energy of the system
α_0	A constant value
δ_d	Debonding failure displacement of strengthened beam
ε_c	Concrete strain at compressive extreme fiber

Department of Civil and Environmental Engineering, Tarbiat Modares University, Tehran, Iran.
*Corresponding Author; E-mail: tasnimi@modares.ac.ir

$\varepsilon_{c,1}$ Concrete strain at compressive extreme fiber, before debonding failure
$\varepsilon_{c,2}$ Concrete strain at compressive extreme fiber, after debonding failure
ε_s Strain in tensile rebar
$\varepsilon_{s,1}$ Strain in tensile rebar, before debonding failure
$\varepsilon_{s,2}$ Strain in tensile rebar, after debonding failure
$\varepsilon'_{s,1}$ Strain in compressive rebar, before debonding failure
$\varepsilon'_{s,2}$ Strain in compressive rebar, after debonding failure
ε_y Yield strain of rebar
ε^p Plastic strain of rebar
θ Mode mixity
$\boldsymbol{\xi}$ Displacement
$\boldsymbol{\sigma}$ Normal stress
φ Curvature of section
φ_1 Curvature of section, before debonding failure
φ_2 Curvature of section, after debonding failure
Δ_{dc} Deflection of strengthened beam at load points, after debonding failure
Δ_{ds} Deflection of strengthened beam at load points, before debonding failure
$\mathbf{E}_{pot}$ Potential energy of the system
$\mathbf{\Phi}(\xi)$ External work due to prescribed surface forces
$\mathbf{\Phi}^*(\sigma)$ External work due to prescribed displacements
Ω Boundary of the system
$\partial\Omega$ System domain

1. Introduction

Use of fiber reinforced polymer (FRP) composites to strengthen reinforced concrete (RC) elements has grown in popularity and established itself as an acceptable technique in repairing and rehabilitating the existing structures in recent decades. The properties which make FRP ideal for structural rehabilitation include their high strength to weight ratio, corrosion resistance and the ease with which they can be applied, especially when the structure is in use. Depending on the design objectives, bonding FRP laminates and sheets to the external surfaces of structural members may lead to improvements in structural performance such as load carrying capacity, stiffness, durability and serviceability. The main applications of FRP on RC members are related to shear and flexural reinforcement of beams, and confinement of columns and joints.

RC elements generally fail by either crushing of compressive concrete and/or yielding of internal steel reinforcement. Although carbon fiber reinforced polymers (CFRPs) have high strength, they are brittle. When these materials are loaded in tension, they show a linear elastic stress–strain behavior followed by a brittle failure without a yielding plateau or any indication of an impending failure. In flexural strengthening of beams, CFRP plates are bonded to the tension side of beams. If the bond between concrete and adhesive remains intact, stresses can be transferred from concrete to CFRP, and vice versa, and full composite action between the CFRP plate and RC beam will occur; otherwise, premature debonding occurs, the composite action is lost, and thus the beam cannot reach the theoretical ultimate capacity of the composite beam. If an FRP-strengthened beam retains its composite action, there are two possible failure modes: (1) compressive concrete crushing prior to, or after, tensile steel yielding, and (2) flexural failure due to rupture of the FRP (Saxena et al. 2008). When debonding occurs between FRP and concrete, the composite action of the beam is lost, which is characterized by the following three failure modes.

(1) Plate end (PE) debonding: This kind of debonding initiates at the vicinity of the FRP end and propagates towards the middle of the beam (Achintha and Burgoyne 2013). PE debonding is formed due to the high interface stresses near the ends of the bonded plate. When the stresses exceed the strength of the weakest element, failure occurs. Upon failure, the FRP will debond from the concrete substrate, at one end of the beam leading to failure of the specimen.
(2) Concrete cover separation: This failure mode is formed by crack development at the plate end propagating upwards to the level of the steel tensile reinforcement and horizontally along the reinforcement. The extension of crack along the tensile reinforcement leads to concrete cover separation and the failure of the specimen. This type of failure typically occurs in members with relatively thin cover, large internal reinforcing bars and a strong FRP-concrete interface.
(3) Intermediate crack (IC) debonding: This kind of debonding initiates at a high-moment zone and propagates towards a low-moment zone (Achintha and Burgoyne 2013). When a major flexural or flexural-shear crack is formed in the concrete, the tensile stresses released by the cracked concrete are transferred to the FRP reinforcement. As a result, high local interfacial stresses between FRP and concrete are induced near the crack. As the applied loading increases further, the tensile stresses in FRP and hence the interfacial stresses between FRP and concrete near the crack also increase. When these stresses reach their critical values, debonding initiates at the crack, and then propagates towards one of the FRP ends (Teng et al. 2002; Ceroni et al. 2008). IC debonding is a critical failure mode for relatively slender members with relatively thin FRP strips and is the primary focus of the recent researches (Teng et al. 2003).

Some disagreement in the literature exists regarding the most prominent failure mode of FRP-strengthened beams. Liu et al. (2007) believe the dominant failure mode to be IC debonding, whereas Ceroni and Pecce (2010) claim that failure in many cases is caused by PE debonding and Saxena et al. (2008) point at concrete cover separation as the most common mode of failure. Location of failure along the beam and thickness of concrete cover detached depends on several parameters such as cracking pattern, amount of steel reinforcement, presence of steel stirrups, loading scheme and

interaction between shear and normal bond stresses along the interfaces (Yao and Teng 2007; Seracino et al. 2007). It was found that the use of anchorage techniques, such as U-shaped and L-shaped jackets and steel bolts, could be very useful in avoiding or postponing the plate end interfacial debonding and cover separation failure, and to achieve relevant increasing in strength and ductility, but IC debonding of FRP still occurred.

Due to the premature and brittle nature of debonding failures, properly understanding these failures and developing design procedures that properly consider debonding problems are needed to insure the safety and reliability of FRP-strengthened members. This paper presents an experimental and analytical study aiming at better understanding the debonding failures of RC beams externally strengthened using FRP composites, and finally proposes a predictive model for the FRP debonding failure load as a basis for design of these systems.

2. The Experimental Study

The experimental study presented herein is part of a comprehensive experimental research program carried out to investigate the flexural performance and failure modes of FRP-strengthened RC beams under monotonic and reverse cyclic loadings. A limited number of experimental results that are used in the analytical study are provided in this paper. This section presents the results of flexural tests carried out on nine RC beam specimens, with dimensions of 150 mm width, 200 mm height and 1800 mm length. Figure 1 illustrates the geometrical dimensions and reinforcing details for all specimens.

Three of the nine specimens were control beams with no FRP strengthening (CM1, CM2 and CC), and the remaining six beams were externally strengthened by CFRP laminates and sheets in flexure and flexure-shear, with and without anchoring of the CFRP laminates used for flexure. Of the six strengthened beams presented in this paper, three specimens (S1-group beams) were strengthened in flexure only (S1 MN, S1M and S1C), and the remaining three specimens (S2-group beams) were strengthened in flexure and shear (S2M1, S2M2 and S2M3). All beams were strengthened in flexure using two unidirectional CFRP laminates 1.2 mm thick, 50 mm wide and 1550 mm long, externally bonded to the soffit and top of the beam. Shear strengthening of S2-group beams was performed along the half shear span using side-bonded 50 mm wide straight CFRP laminates (S2M1), side-bonded 200 mm wide straight CFRP sheets (S2M2), and wrapped 200 mm wide CFRP sheet (S2M3). All beams had the plate end anchorage by wrapped 50 mm wide CFRP sheet, except the first specimen (S1MN). The strengthening configurations and the related parameters are provided in Fig. 2 and Table 1, respectively.

The concrete used for all specimens was a normal strength concrete cast in the laboratory. Two different grades (with mean yield strengths of 400 and 600 MPa) of steel rebar of 16 mm in diameter were used in the test beams for longitudinal reinforcement. The stirrups of Φ8 with yield strength of 400 MPa were placed as shown in Fig. 1. The elastic modulus of all reinforcement (rebar and stirrups) was 200 GPa. Tables 2 and 3 summarize the properties of all materials used in the experimental study.

All beams were tested in a four-point bending, because it gives constant maximum moment and zero shear in the section between the loads. The loading was applied as displacement-controlled monotonic or quasi-static cyclic loading history by a reversible two-point loading system located at 275 mm on either sides of the mid-span. Monotonic loading was applied with a constant rate of 0.1 mm/s, until the beam failed. During cyclic loading, the beams were loaded at a constant rate of 0.1 mm/*sec* and unloaded at 0.5 mm/s, according to the loading protocol shown in Fig. 3. Quasi-static cyclic loading history consisted of two phases. The first phase was force-control and the second phase was displacement-control. The first phase of loading was comprised of two cycles which imposed a force corresponding to 50 % of the theoretical strength of the test specimen. At the early stage of the second phase of loading, one fully reversed cycle with equal amplitude of 100 % of the yield displacement was applied. This phase was followed by several subsequent parts, each containing two fully reversed cycles of equal amplitude, corresponding to 200, 300, 400 and 600 % of the yield displacement.

All specimens were loaded using a hydraulic jack of 600 kN capacity and maximum stroke of ± 100 mm. A load cell was used to record applied loads. Figure 4 shows the schematic testing setup. Three linearly variable differential transducers (LVDTs) were positioned at the mid-span and the load points, to measure the deflection during each test.

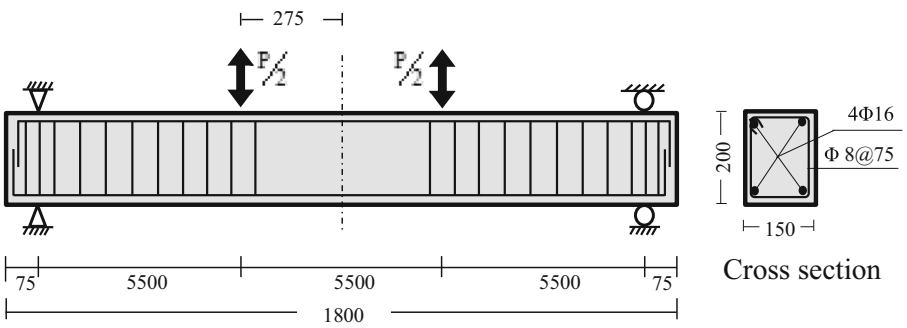

Fig. 1 Geometric dimensions and reinforcement of the tested beams (Unit: mm).

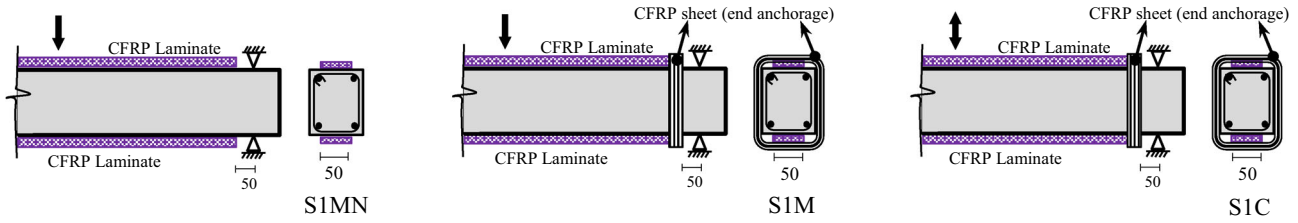

(a) S1-group beams: Beams strengthened in flexure

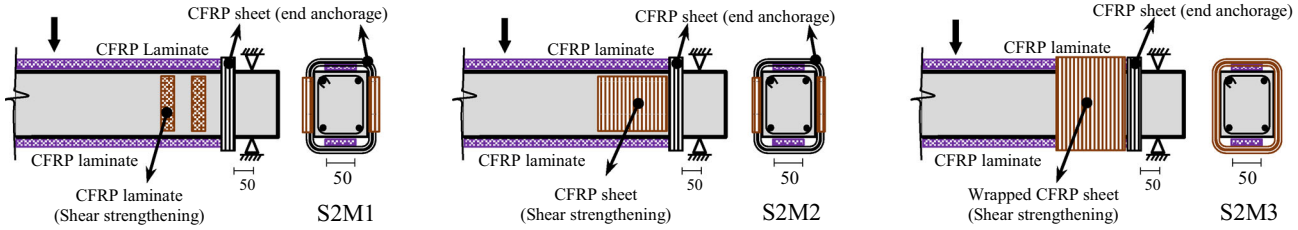

(b) S2-group beams: Beams strengthened in flexure and shear

Fig. 2 Strengthening configurations of specimens. **a** S1-group beams: Beams strengthened in flexure **b** S2-group beams: Beams strengthened in flexure and shear.

Table 1 Strengthening parameters for specimens.

Specimens		Label	Loading history	Flexural strengthening with CFRP laminate			End anchorage	Shear strengthening with CFRP laminate/sheet	
				w_f (mm)	t_f (mm)	L_f (mm)		w_f (mm)	Type (laminate or sheet)
Control beams		CM1	Monotonic	–	–	–	–	–	–
		CM2	Monotonic	–	–	–	–	–	–
		CC	Cyclic	–	–	–	–	–	–
Strengthened beams	S1-group	S1 MN	Monotonic	50	1.2	1550	No	–	–
		S1M	Monotonic	50	1.2	1550	Yes (EA)	–	–
		S1C	Cyclic	50	1.2	1550	Yes (EA)	–	–
	S2-group	S2M1	Monotonic	50	1.2	1550	Yes (EA)	50	Laminate (t = 1.2 mm)
		S2M2	Monotonic	50	1.2	1550	Yes (EA)	200	Sheet
		S2M3	Monotonic	50	1.2	1550	Yes (EA)	200	Wrapped Sheet

S1 Beams strengthened in flexure only; *S2* Beams strengthened in flexure and shear; *EA* End anchorage by wrapped CFRP sheet of 50 mm wide.

Table 2 Concrete and steel rebar properties (MPa).

Specimens	Label	Concrete compressive strength			Steel yield strength		
		Number of samples	Mean $\mu(f'_c)$	Standard deviation $\sigma(f'_c)$	Number of samples	Mean $\mu(f_y)$	Standard deviation $\sigma(f_y)$
Control beams	CM1	6	30.2	2.7	3	400.1	1.9
	CM2	6	38.7	2.1	3	598.9	2.4
	CC	6	40.6	3.1			
Strengthened beams	S1C	6	39.6	3.7	3	600.6	2.7
	S1 M	6	40.7	1.5			
	S1MN	6	32.7	2.6	3	399.7	2.1
	S2M1	6	40.5	3.1			
	S2M2	6	37.5	1.9			
	S2M3	6	33.8	1.0			

Table 3 Properties of materials used for strengthening (MPa).

Material	Tensile strength	Shear strength	Elastic modulus
CFRP laminate	3420	–	171,600
Epoxy adhesive[1]	49.5	25	4500
CFRP Sheet[a,b]	4194	–	226,100
Resin[a]	49.8	–	3200

[a] The properties were provided by the manufacturer.

[b] The properties of CFRP sheet have been reported based on the net fiber area.

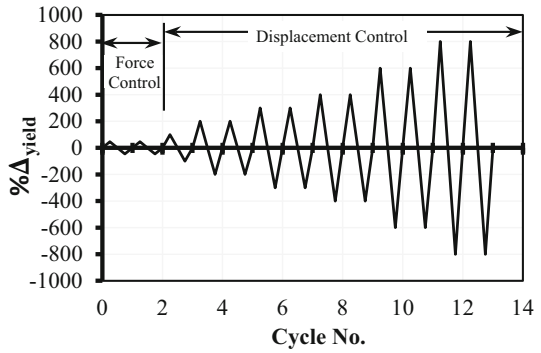

Fig. 3 Cyclic loading protocol (Filiatrault et al. 2008).

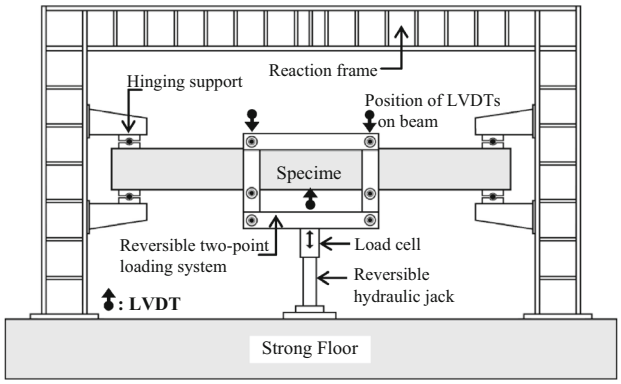

Fig. 4 Schematic testing setup.

The output data including applied load and deflections were recorded during the test by a computer data logger system.

Figure 5 shows load–deflection curve of control beams CM1, CM2 and CC tested under monotonic, monotonic and cyclic loadings, respectively. The load carrying capacity of monotonic control beams CM1 and CM2 were 114 and 135 kN, respectively. The difference in load capacity of these beams can be attributed to the change in rebar grade and properties of concrete used (see Table 2). The load–deflection curves of CC and CM2 specimens show the same behavior, but a slight difference in load capacity and ductility are observed (Fig. 5b). The control beams failed by typical steel yielding followed by concrete crushing, and showed wide flexural cracks at mid-span that extended to the compression area.

The load–deflection response for the beams strengthened with CFRP laminates and sheets, and tested under monotonic and cyclic loadings are shown in Fig. 6. The load carrying capacity of monotonic beams strengthened in flexure (S1 MN and S1 M) were 123 and 150 kN, respectively. S1 MN and S1 M specimens are the strengthened beams corresponding to the control beams CM1 and CM2, respectively. Therefore, behavior of S1 MN and S1 M was compared with that of their respective control beams CM1 and CM2. As shown in Figs. 6a and 6b, the load carrying capacity of beams S1 MN and S1M was increased in comparison with their respective control beams (CM1 and CM2), until the debonding failure occurred. After debonding failure, beam S1M shows a behavior similar to CM2, and beam S1MN behaves as a beam with less strength than CM1. A close observation from Fig. 6 is that while the load carrying capacity of beam S1M was increased by 12 % higher than that of the control beam CM2 (Fig. 6b), the load carrying

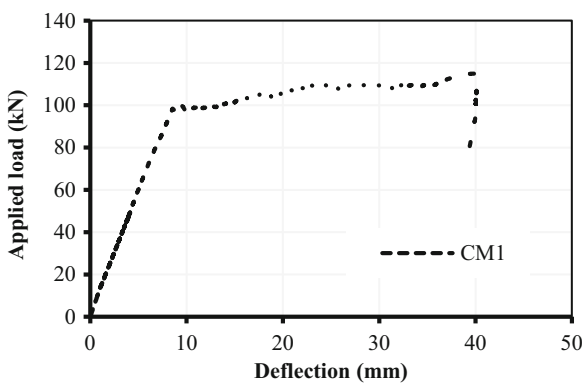

(a) Control beam CM1

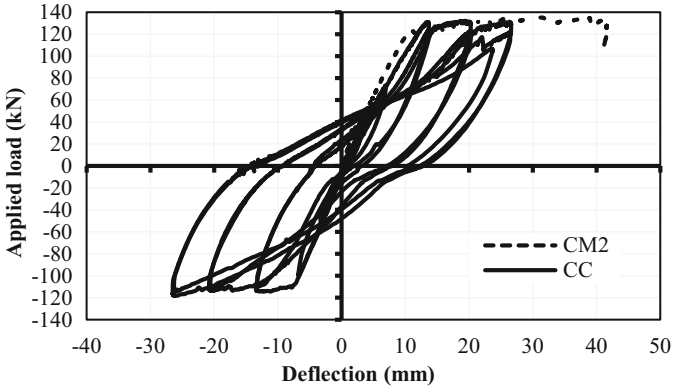

(b) Control beams CM2 and CC

Fig. 5 Load-deflection curve of control beams.

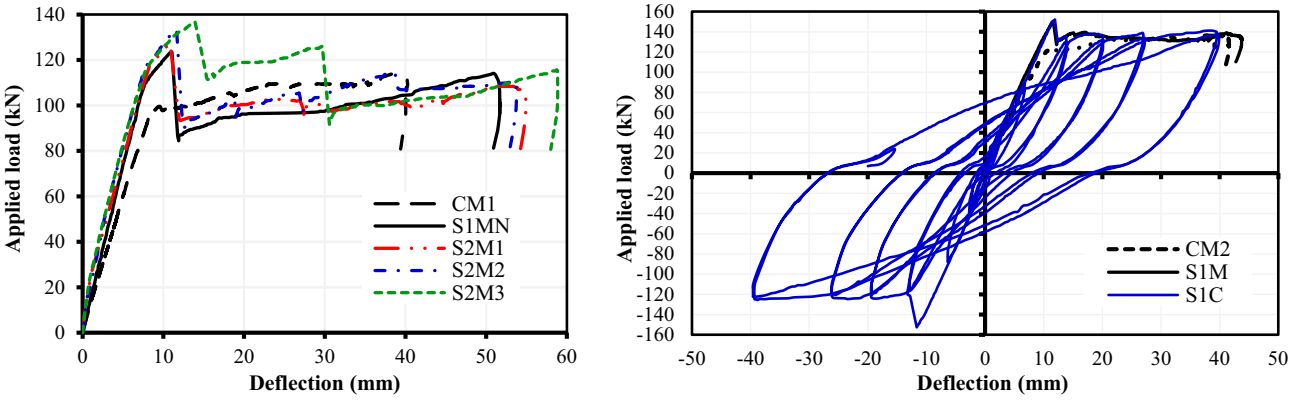

(a) S1MN, S2M1, S2M2 and S2M3 specimens in comparison with their relevant control beam CM1

(b) S1M and S1C specimens in comparison with their relevant control beam CM2

Fig. 6 Load-deflection curve of strengthened beams.

capacity of beam S1MN was increased by about 8 % higher than that of the control beam CM1 (Fig. 6a). The lower increase in the load carrying capacity of beam S1MN is due to the premature failure of this specimen through end debonding of tensile CFRP laminate. The failure mode of beam S1MN was plate-end debonding that occurred at the right end of tensile laminate, followed by complete debonding of tensile CFRP laminate. Finally, this beam was failed because of the crushing of compressive concrete (flexural failure mode). The debonding failure mode of beam S1M was the interfacial debonding of tensile laminate induced by flexural-shear cracks formed in the right shear span of the beam, followed by the buckling of compressive CFRP laminate, and finally, by the crushing of compressive concrete.

S2M1, S2M2 and S2M3 specimens were strengthened in both flexure and shear, and were tested under monotonic loading. The load capacity of strengthened beams S2M1, S2M2 and S2M3 were 127, 133 and 137 kN, respectively. Wrapping of the beam S2M3 by CFRP sheet resulted in more increasing of load capacity in comparison with the other specimens of S2-group (S2M1 and S2M2). As shown in Fig. 6a, the load carrying capacity of beams S2M1, S2M2 and S2M3 was increased 3, 8 and 11 % higher than that of the strengthened beam S1MN, until the debonding of tensile laminate occurred. After that, a behavior similar to S1MN was shown for beams S2M1 and S2M2; while the beam S2M3 behaved as a beam with more strength than S1MN, until the debonding of compressive laminate occurred, and then showed a behavior similar to S1MN. Although S2M1 and S2M2 specimens showed a significant load drop of 33 and 43kN occurred in one step, the beam S2M3 showed significant load drops of 24 and 39 kN occurred in two steps. Then, as can be seen from Fig. 6a, wrapping of the strengthened beams by CFRP sheet (S2M3) can result in better performance of specimen. The failure mode of beam S2M1 was interfacial debonding of tensile laminate induced by flexural crack formed in the beam mid-span, followed by the debonding and buckling of the bottom CFRP. The failure mode of beam S2M2 was interfacial debonding of tensile laminate induced by flexural-shear crack formed in the left shear span, followed by the partial debondings and finally the buckling of compressive CFRP laminate. The beam S2M3 failed due to initiation and propagation of the interfacial debonding of tensile laminate induced by flexural-shear crack formed in the right shear span (region close to the right load position). These cracks propagated towards the right end of tensile laminate, followed by rupture of end anchorage which occurred along the right shear span of the beam, and resulted in complete debonding of tensile CFRP laminate and the buckling of compressive CFRP laminate.

The load–deflection curve of the two identical FRP-strengthened beams tested under monotonic (S1 M) and cyclic (S1C) loadings are shown in Fig. 6b. As shown in this figure, the behavior and characteristics of the two beams are nearly identical, as the backbone of load–deflection curve of specimen S1 M appears as the envelope curve for the load–deflection curve of specimen S1C. It should be noted that the beam CC is the cyclic control beam corresponding to the cyclic strengthened beam S1C. The increase in load capacity of S1C, compared with that of the beam CC, was 15 %. The failure mode of beam S1C was the interfacial debonding of CFRP laminates, followed by complete debonding of top and bottom CFRP laminates. For the cyclic strengthened specimen (S1C), the debonding of top and bottom laminates occurred in upward and downward 4th cycles of load, respectively. The debonding of top laminate initiated from the location of close to the left load position, and propagated towards the left end of the beam and the mid-span, while that of the bottom laminate initiated at the mid-span, and propagated towards both ends of beam.

3. Analytical Model of FRP Debonding

Although the fracture process of the FRP-strengthened beams is gradual and stable in initial steps of loading, upon reaching a critical energy state, the debonding failure occurs; which results in the energy transformations in the system. “In order to study the energy variation of a FRP strengthened

beam during loading steps, energy balance equation was used.

Considering the energy balance in FRP-strengthened beam, the irreversible energy dissipation of the system, **D**, can be written as (Ulm and Coussy 2001):

$$dD = dW^{ext} - dW \tag{1}$$

in which, $\mathbf{W}^{ext}$ and **W** are the total external work and the free energy of the system, respectively. Equation (1) indicates that the amount of externally supplied work, not stored in the system as free energy, is dissipated in the system. In the absence of inertia and body forces, the total external work, $\mathbf{W}^{ext}$, of the system with domain Ω and boundary ∂Ω can be obtained from the theorem of virtual work, as follows:

$$W^{ext} = \int_{\partial\Omega} T.\,\xi\, dA \tag{2}$$

where **T** denotes surface tractions acting at boundary of the system. The externally supplied work in Eq. (2) can be separated into two parts as the external work due to prescribed surface forces, $\mathbf{\Phi}(\xi)$, and the external work due to prescribed displacements, $\mathbf{\Phi}^{*}(\sigma)$, as follows:

$$W^{ext} = \Phi(\xi) + \Phi^{*}(\sigma) \tag{3}$$

Combining Eqs. (1) through (3), and introducing the potential energy of the system, $\mathbf{E}_{pot}$, in the following form (Buyukozturk et al. 2002):

$$\mathrm{E}_{pot} = W - \Phi \tag{4}$$

the expression for total energy dissipation in Eq. (1) can be rewritten, for constant prescribed surface forces and displacements, as follows: ($d\mathbf{D} \approx \Delta\mathbf{D}$, $d\mathbf{E}_{pot} \approx \Delta\mathbf{E}_{pot}$)

$$\Delta D = -\Delta \mathrm{E}_{pot} \tag{5}$$

Thus, this equation gives the total energy dissipation during debonding as the negative change in the potential energy of the system. In order to establish a criterion for FRP debonding based on Eq. (5), it is necessary to determine the terms of the right and left hand sides of Eq. (5).

The term of right hand side of Eq. (5), $\Delta\mathbf{E}_{pot}$, states the total change in the potential energy of the system during debonding, which equals to the difference between the recoverable energy stored in the beam before and after debonding. The potential energy difference between strengthened and debonded states of FRP-strengthened beams is graphically shown in Fig. 7. Once debonding failure occurs, the strengthened beam (shown with solid line) is assumed to behave as an un-strengthened beam (shown with thick dashed line). According to Buyukozturk et al. (2002), the difference in the potential energy of the beam, before and after debonding is illustrated by the shaded area.

As can be seen from Fig. 7, the change in potential energy can be calculated through the load–deflection curves of the strengthened and control (unstrengthened) beams. These load–deflection curves have been idealized based on the bilinear load–displacement relationship, and the equal stiffness of unloading and pre-yielding stages. It should be noted that Fig. 7 is based on assuming the beam deflection and curvature stay constant upon debonding, which includes a significant error in predicting the load of debonding failure. The results of the present tested specimens and other test results (Ceroni and Pecce 2005; Esfahani et al. 2007; Ceroni 2010; Obaidat et al. 2011; Spadea et al. 2015) indicate that the beam deflection and thus the curvature increases during debonding failure from Δ_{ds} to Δ_{dc}. Detailed explanation is given in Sect. 3.1. Therefore, the difference in the potential energy of the beam, before and after debonding, can be indicated by the shaded area shown in Fig. 8.

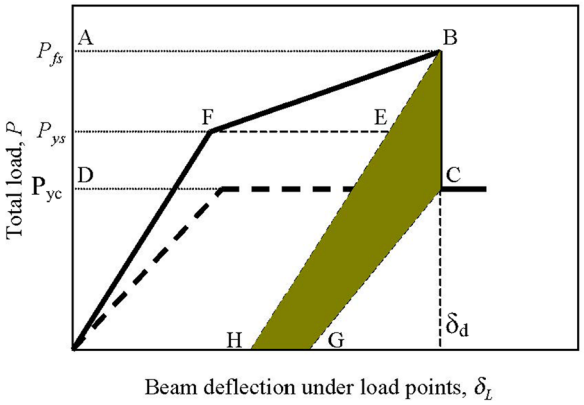

Fig. 7 Potential energy difference in the beam upon debonding failure (Buyukozturk et al. 2002).

Considering the increase in beam deflection during debonding failure, the change in the potential energy of the beam, before and after debonding, ($\Delta\mathbf{E}_{\mathrm{pot}}$) is obtained as below (Fig. 8):

$$\Delta E_{pot} = \frac{P_{ds}^2}{2K_s} - \frac{P_{dc}^2}{2K_c} + \frac{\delta\Delta_d}{2}(P_{ds} + P_{dc}) \tag{6}$$

in which, $\delta\Delta_d = \Delta_{dc}$—$\Delta_{ds}$; Δ_{ds} and Δ_{dc} are the deflection of the strengthened beam at load points, before and after debonding failure, respectively; $P_{ds} = P(\Delta = \Delta_{ds})$ and $P_{dc} = P(\Delta = \Delta_{dc})$ are the load values for before and after debonding failure, respectively; and K_s and K_c are the stiffness of the strengthened and control beams respectively, which in the case of a beam tested in four-point bending can be expressed by (Gunes et al. 2006):

$$K_s = 2EI_s \Big/ \left(\frac{L}{2}l_s^2 - \frac{2}{3}l_s^3\right) \quad , \quad K_c = 2EI_c \Big/ \left(\frac{L}{2}l_s^2 - \frac{2}{3}l_s^3\right) \tag{7}$$

where I_s and I_c are the moments of inertia of the transformed sections in cracked condition, before and after debonding failure, respectively. Having established the potential energy difference of the beam during debonding ($\Delta\mathbf{E}_{pot}$), it requires to determine the term of left hand side of Eq. (5), $\Delta\mathbf{D}$, which states the total energy dissipation of the beam during debonding failure.

The total energy dissipation ($\Delta\mathbf{D}$) in FRP-strengthened beams under loading occurs due to the various mechanisms

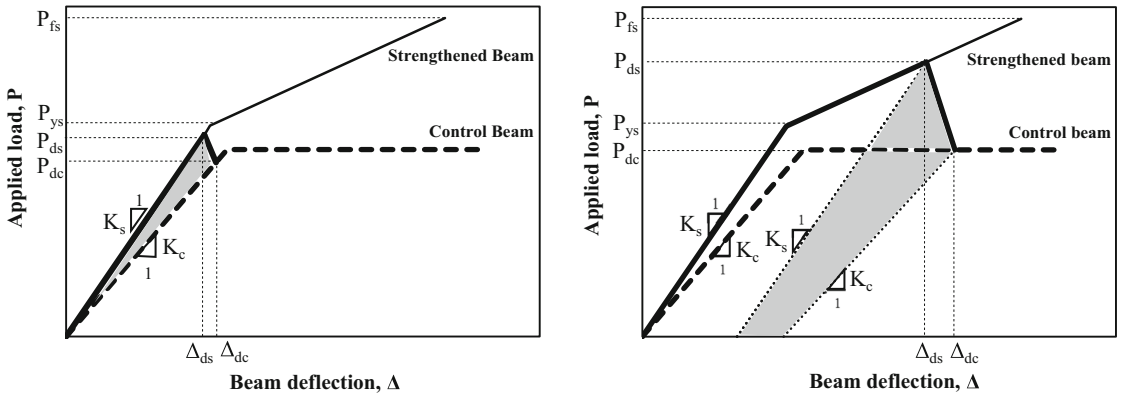

(a) debonding failure before rebar yielding **(b)** debonding failure after rebar yielding

Fig. 8 Energy dissipation during debonding failure.

such as concrete cracking, rebar yielding and FRP debonding. Considering the various experimental observations, the energy dissipation within the system due to mechanism of concrete cracking is less significance compared to the other terms, since much of the concrete cracking takes place before debonding. Assuming the energy dissipation due to this mechanism to be insignificant, the dominant modes of energy dissipation are the debonding fracture process and the steel rebar yielding. Thus, the total energy dissipated during debonding failure is equal to the interface fracture energy and a plastic energy term that accompanies the fracture process. Then, the expression for energy dissipation ($\Delta\mathbf{D}$) can be written in general terms as:

$$\Delta D = D^{d}_{FRP} + D^{y}_{st} \tag{8}$$

in which, D^{d}_{FRP} is the energy dissipation due to debonding of FRP laminate, and the term D^{y}_{st} represents the energy dissipation due to yielding of steel rebar. It is obvious that D^{y}_{st} is equal to zero when $\varepsilon_s \leq \varepsilon_y$. Then, debonding failure is not a pure fracture process in FRP-strengthened RC beams, and a term of the energy dissipation due to rebar yielding is included in the expression of energy dissipation ($\Delta\mathbf{D}$). Thus, it is necessary to quantify these two mechanisms for modelling of debonding failure.

3.1 Energy Dissipated due to Rebar Yielding

As shown in Fig. 8, FRP debonding in the strengthened beams may take place before or after rebar yielding, which depends on several parameters such as beam geometry, amount of steel reinforcement and strengthening configuration. To formulate a debonding failure criteria based on Eq. (8), the term of energy dissipation due to yielding of steel rebar (D^{y}_{st}) should be characterized.

Buyukozturk et al. (2002) considered the dissipated energy due to yielding of rebar as a linear function of the failure displacement, and presented an approximate expression as:

$$D^{y}_{st} \approx 3.0\left(P^{\delta_d}_{fs} - P^{\delta_d}_{fu}\right) \tag{9}$$

where $P^{\delta_d}_{fs}$ is the failure load of the strengthened beam at the debonding displacement of δ_d, indicated as point B in Fig. 7, and $P^{\delta_d}_{fu}$ is the load of control beam corresponding to the displacement of δ_d, shown as point C in Fig. 7. Considering that this empirical expression is inadequate, an improved estimation is required that also takes into account the beam geometry and reinforcement. Gunes et al. (2006) assumed that the displacement and thus the curvature of the beam stays constant upon debonding, and derived the term of energy dissipation due to rebar yielding, as follows:

$$D^{y}_{st} = \int \sigma . d\varepsilon^{p} d\Omega = f_y \varepsilon_c (1 - c_2/c_1) A_s l_c \tag{10}$$

in which, $\varepsilon^{p} = \varepsilon_s - \varepsilon_y > 0$, and l_c is the length of the constant moment region.

Although the assumption of constant curvature at debonding was also adopted in the theoretical analysis carried out by Bencardino and Condello (2016), experimental data sets produced by other researchers (Ceroni and Pecce 2005; Esfahani et al. 2007; Ceroni 2010; Obaidat et al. 2011; Spadea et al. 2015), and also the tested beams herein show that assuming the constant deflection and curvature during debonding is not valid and can be resulted in significant error in predicting the load of debonding failure. In contrast with assuming the constant deflection during debonding, the above mentioned results indicate that the deflection and curvature of the beam increases by 7–15 %, during debonding failure. In this research, considering the increase of 10 % in the deflection and thus curvature of the beam during debonding failure (Fig. 8), the energy dissipation term during debonding through yielding of the steel reinforcement can be derived. Figure 9 shows the strain profile in the beam cross-section before and after debonding failure. Using the definition of curvature ($\varphi = \varepsilon_c/c$), considering the strain compatibility as $\varepsilon_s = \varphi\ (d–c)$, and assuming the increase of 10 % in the curvature during debonding failure ($\varphi_2 = 1.1\varphi_1$), the change in rebar strain upon debonding is given by:

$$\Delta\varepsilon_s = \varepsilon_{s,2} - \varepsilon_{s,1} = \varepsilon_c(1 + 0.1d/c_1 - 1.1\, c_2/c_1) \tag{11}$$

Using Eq. (11), the term of energy dissipation due to rebar yielding during debonding failure can be determined by:

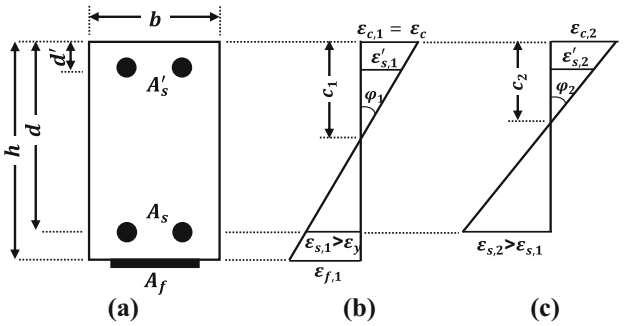

Fig. 9 Strain profile across beam section: **a** beam cross-section, **b** strain distribution before debonding, and **c** strain distribution after debonding.

$$D_{st}^{y} = \int \sigma . d\varepsilon^{p} d\Omega = \sigma_s \Delta\varepsilon_s A_s l_s = f_y \varepsilon_c (1 + 0.1d/c_1 - 1.1c_2/c_1) A_s l_c \quad (12)$$

where all notations are depicted in Fig. 9. Subscripts 1 and 2 denote quantities for before and after debonding failure, respectively. This term of energy dissipation equals zero when $\varepsilon_s \leq \varepsilon_y$.

3.2 Energy Dissipated due to FRP Debonding

As stated previously, the term of energy dissipation due to FRP debonding (D_{FRP}^{d}) is an important part of Eq. (8) which evaluated over the interface crack surface. This term of energy dissipation is defined by the energy per unit area necessary for the crack formation, called the bond fracture energy (G_f), and the interfacial bond area (A_f), as follows:

$$D_{FRP}^{d} = \int G_f dA_f \quad (13)$$

The portion of the energy of the system, which dissipated at the FRP-concrete interface upon debonding, causes to create the new fracture surfaces along the bond area. Depending on the fracture properties of the materials, the debonding may occur within or at the interfaces of the materials.

A crack in a material can propagate either by opening (mode-I), shearing between the two crack faces (mode-II), or by a combination of both (mixed-mode). In different modes of fracture, different stress-displacement fields will develop in the vicinity of the crack, so the fracture energy depends on which fracture mode occurs (Achintha and Burgoyne 2013). Although in the case of brittle, isotropic and homogeneous solids, cracks propagate by maintaining pure mode-I condition at the crack tip, the stress field that triggers debonding at an interface can be very complex (Hutchinson and Suo 1992). Various forms of stress concentrations develop due to different fracture energies of two joining materials and also due to the number of geometric constraints present in the vicinity. Thus, it would be expected that interface cracks are governed by mixed-mode effects. An interface crack under mixed-mode loading can experience either kinking or straight-ahead propagation, depending on the relative fracture resistances associated with the competing possible directions of advance (Hutchinson and Suo 1992). In straight-ahead propagation case, the interface is relatively weaker than the bordering materials, meaning that the interface crack propagates along the least resistance path, interface. In the crack kinking case, the interface is relatively tougher than at least one of two adjoining materials (Li et al. 1995).

The mixed-mode fracture energy of interface depends on the respective fracture energies of pure primary modes ($G_{F,I}$ and $G_{F,II}$) and also on the magnitude of the component of each primary mode of fracture involved during a unit total extension of the crack (Hutchinson and Suo 1992). The relative contributions of each primary mode is nominated "mode mixity", θ, which defined as the ratio of the components of mode-II to mode-I. The mixed-mode interface fracture energy usually increases with the increase of θ, since $G_{F,II}$ is often higher than $G_{F,I}$. In linear elastic fracture mechanics, the mode mixity (θ) is defined as:

$$\tan\theta = \sqrt{G_{F,II}/G_{F,I}} \quad (14)$$

So, the bond fracture energy G_f in Eq. (13) can be expressed as:

$$G_f = G_F(\theta) \quad (15)$$

in which, the mixed-mode fracture energy of the interface $G_F(\theta)$, can be regarded as an effective surface energy that depends on the mode mixity θ; where $\theta = 0$ and 90° correspond to pure mode-I and mode-II fractures, respectively. To accurately predict the debonding behavior of an externally FRP-strengthened RC beam, the concrete substrate and both concrete-adhesive and FRP-adhesive interfaces must be considered. Methods dealing with mixed-mode fracture of layered materials can account for the fracture properties of the interfaces and substrate materials and can be used to determine the debonding propagation path that may occur along the FRP-concrete interface or within the concrete. Most researchers assumed that the debonding crack propagates only along the FRP-concrete interface or within the concrete substrate. However, Hearing and Buyukozturk (1997) modeled the FRP debonding as a crack that initiates within the concrete-adhesive interface and then propagates along the interface or into each of the substrates. Gunes et al. (2006) considered the debonding as a crack that propagates along the concrete-adhesive interface and does not diverge into the substrates. Also, they assumed that the mixed-mode fracture energy converges rapidly to the mode-II value at high phase angles due to friction and asperity effects such as surface roughness; and thus emphasized that the debonding can be regarded as mode-II fracture of concrete-adhesive interface.

Although most models of FRP debonding are based on mode-II fracture energy of the bonded system which is mostly determined by simple shear tests, experimental observations and results confirm that the concrete substrate just above the interface is the most likely place for failure to occur. Also, the experimental results confirm that concrete

cracking initiates as a mode-I fracture; especially when adhesives recommended by FRP manufacturer are used with appropriate curing procedures. It is also considered in many experimental research that the debonding failure occurs in concrete at a few millimeters from the FRP-concrete interface and is essentially parallel to the interface. This phenomenon is because of two reasons: first, the penetration of adhesive into the concrete, and the increase in toughness and strength of a thin layer of mortar just next to the interface; and second, the concrete substrate is the weakest component in FRP-concrete interface which has a relatively small tensile strength (Coronado and Lopez 2008). Thus, the debonding behavior is mostly related to the concrete properties, and concrete cracking initiates as a mode-I fracture.

Briefly, studies of most researchers have shown that:

(1) Although the interface of a strengthened beam is primarily carrying shear, it actually fails in tension. Thus, FRP debonding propagates locally as a mode-I fracture in concrete (Achintha and Burgoyne 2011, 2013).
In both cases of PE and IC debondings, the debonding occurs within the concrete substrate, adjacent to the interface; and meanwhile, the effects of mode-I are dominant in the debonding propagation. The whole concrete cover of the beam usually separates during PE debonding, whereas a concrete layer of only a few millimeters thick separates during IC debonding (Achintha and Burgoyne 2012).

(2) Because of the relatively high shear fracture resistance of concrete, it has been widely assumed that a crack under mixed-mode loadings propagates by opening of the crack tip, although the direction of propagation depends on the mode mixity. It has been further derived that a crack starts to open when the maximum principal tensile stress (MPTS) at the crack tip reaches f_{ct}, and instantaneous propagation will be in the direction perpendicular to that of the MPTS. Thus, it is appropriate to assume that the crack opening will be associated with the same fracture energy as that under pure mode-I. This assumption has been widely validated in the literature (Galvez et al. 1998).

(3) Single/double shear-lap experiments, which commonly used in the literature to determine the parameters for the analysis of FRP debonding, do not provide meaningful fracture parameters that can be used in the analysis; because the tests provide an estimate of mode-II fracture energy whereas a mode-I fracture triggers debonding. Fracture energy values derived from the tests ($G_{C,II}$) were significantly higher than that against FRP debonding (Achintha and Burgoyne 2012, 2013).

(4) Some recent studies have experimentally investigated the mode-I fracture energy in the vicinity of concrete-FRP interface, and shown that the fracture energy calculated is of similar magnitude to that of pure concrete. The results illustrated that if the failure takes place within the concrete, the presence of nearby FRP does not affect fracture energy $G_{C,I}$ (Achintha and Burgoyne 2013, Qiao and Xu 2004).

(5) Manufacturers have now developed sufficiently tough adhesives that, if used correctly, failure usually takes place in the concrete just above the interface. Thus, it is possible to assume that the interface fracture energy, G_F, is the same as the fracture energy of concrete, G_C (Achintha and Burgoyne 2012, 2013).

Regarding the above discussions, in this research, the FRP debonding is assumed to propagate as a mode-I fracture of concrete; thus, the fracture energy of the FRP-concrete interface is equal to mode-I fracture energy of concrete. Experimental observations during tested beams have also revealed that debonding at the FRP–concrete interface generally occurs within concrete, at a few millimeters from the FRP-concrete interface as parallel to the interface; while debonding of end anchorage takes place at the FRP–FRP interface as a mode-II fracture. Thus, the associated fracture energies can be considered as:

$$G_f = G_C(\theta) \approx G_{C,I} \quad : \text{flexural FRP laminate} - \text{concrete interface} \tag{16}$$

$$G_f = \bar{G}_F(\theta) \approx \bar{G}_{F,II}\text{: flexural FRP laminate} - \text{FRP end anchorage interface} \tag{17}$$

in which, $G_C(\theta)$ and $G_{C,I}$ are the mixed-mode and mode-I fracture energies of concrete; $\bar{G}_F(\theta)$ and $\bar{G}_{F,II}$ are the mixed-mode and mode-II fracture energy of the interface between the flexural FRP laminate and wrapped FRP sheet (end anchorage). Now, by assuming that debonding occurs along the entire bond area between the flexural FRP reinforcement and concrete, the term of the debonding energy dissipation (Eq. (13)) can be rewritten as:

$$D^d_{FRP} = G_{C,I}(l_f . w_f) + \bar{G}_{F,II}(l_a . w_a) \tag{18}$$

where $l_f.w_f$ is the bond area at interface between the flexural FRP laminate and concrete, and $l_a.w_a$ is the bond area between the flexural FRP laminate and the wrapped FRP sheet (end anchorage). To determine the term of energy dissipation due to FRP debonding process (Eq. (18)), it requires the knowledge of the fracture energies of $G_{C,I}$ and $\bar{G}_{F,II}$.

Achintha and Burgoyne (2013) tested and discussed the performance of several models of mode-I fracture energy of concrete, including empirical or analytical models of Gustafsson and Hillerborg (1985), Reinhardt (1985), Guinea et al. (1994), CEB-FIP code (1991), and Bazant and Becq-Giraudon (2001). Achintha and Burgoyne (2013) showed that the estimations from all models, but the CEB-FIP code (1991) which underestimates $G_{C,I}$, give predictions that match well with values to be expected from tests; and found that among these models, the empirical model of Bazant and Becq-Giraudon is the best that precisely estimates the mode-I fracture energy of concrete ($G_{C,I}$). Thus, model of Bazant and Becq-Giraudon (2001) was used in this research as the

selected model, which considers the mode-I fracture energy of concrete, $G_{C,I}$, as below:

$$G_{C,I} = 2.5\alpha_0 \left(f_c'/0.051\right)^{0.46} (1 + d_{a-\max}/11.27)^{0.22} (w/c)^{-0.30} \tag{19}$$

in which, $\alpha_0 = 1$ and 1.44 for rounded and crushed aggregates respectively. In this research, $\alpha_0 = 1.44$, $w/c = 0.47$, and $d_{\text{a-max}} = 12.5$ mm. So, the mode-I fracture energy of concrete is obtained based on the compressive strength of cylindrical concrete samples.

Knowledge of mode-II fracture energy of the interface between the flexural FRP laminate and FRP end anchorage ($\bar{G}_{F,II}$) is virtually very limited at this time. Gunes et al. (2006) stated that the value of $\bar{G}_{F,II}$ is higher than that of $G_{F,II}$, and assumed to be twice the Mode-II fracture energy of the FRP-concrete interface ($G_{F,II}$). Due to lack of measured values of $\bar{G}_{F,II}$, it is assumed to be the same as that used by Gunes et al. (2006). Thus, $\bar{G}_{F,II}$ was assumed to be twice the fracture energy $G_{F,II}$ until further research into this parameter reveals more reliable values.

$$\bar{G}_{F,II} = 2G_{F,II} \tag{20}$$

in which, $G_{F,II}$ is determined as:

$$G_{F,II} = 0.122 k_b^2 \sqrt{f_c'} \tag{21}$$

where k_b is a geometric factor that considers the influence of the laminate width (w_f) relative to the width of the concrete member (w_c) according to the following expression:

$$k_b = \sqrt{1.125 \frac{2 - w_f/w_c}{1 + w_f/400}} \tag{22}$$

3.3 Debonding Failure Model

Using Eqs. (5), (6), (8), (12), and (18) through (22), an improved debonding criterion can be developed, which based on bilinear assumption for the beam load–deflection curves, as follows:

$$\frac{P_{ds}^2}{2K_s} - \frac{P_{dc}^2}{2K_c} + \frac{\delta\Delta_d}{2}(P_{ds} + P_{dc}) = (G_{C,I}\, l_f w_f + \bar{G}_{F,II}\, l_a w_a) + f_y \varepsilon_c (1 + 0.1d/c_1 - 1.1c_2/c_1) A_s l_c \tag{23}$$

Equation (23) indicates that upon debonding failure, the portion of energy of the system dissipates through debonding fracture and yielding of the steel rebar. Furthermore, as shown in Fig. 8, in the case of debonding failure after rebar yielding, $P_{\text{dc}} = P_{\text{yc}}$, and thus, Eq. (23) can be simplified as below; where P_{yc} is the load capacity of the control beam at rebar yielding.

$$\frac{P_{ds}^2}{2K_s} - \frac{P_{yc}^2}{2K_c} + \frac{\delta\Delta_d}{2}(P_{ds} + P_{yc}) = (G_{C,I}\, l_f w_f + \bar{G}_{F,II}\, l_a w_a) + f_y \varepsilon_c (1 + 0.1d/c_1 - 1.1c_2/c_1) A_s l_c \tag{24}$$

where the debonding failure load (P_{ds}) can be determined through iteration and trial and error.

4. Validation of the Model

In order to validate the developed model, the model was implemented to predict the load of FRP debonding for the beam tests presented in the Sect. 2; then predictions of the model were compared with the experimental results. Figure 10 indicates the experimental results obtained from the typical beam tests; and also the bilinear load–deflection curves for the strengthened and control beams, which shown with the dashed lines in the figure. These idealized bilinear curves were used as a basis for determination of the debonding failure loads according to Eq. (24). In Fig. 10, the envelope of the load–deflection curve of the cyclic beam S1C has been presented along with the load–deflection curve of the monotonic beam S1 M. As indicated in Fig. 10, the debonding failure in the beams S1MN, S2M1, S2M2 and S2M3 occurred after rebar yielding (Fig. 10a), while the debonding failure in the beams S1 M and S1C occurred before rebar yielding or simultaneously with each other (Fig. 10b).

Figure 11 compares the debonding model predictions with the test results, which indicates that the model yields a satisfactory prediction of the loads of FRP debonding failure. As can be seen from Fig. 11, the proposed model is able to precisely predict the loads of debonding failure in FRP-strengthened RC beams. In order to compare the precision of the proposed model with Gunes et al. (2006) model, the

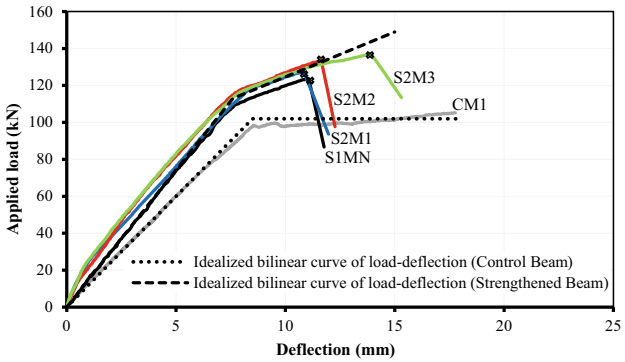

(b) Results of the strengthened beams S1MN, S2M1, S2M2 and S2M3

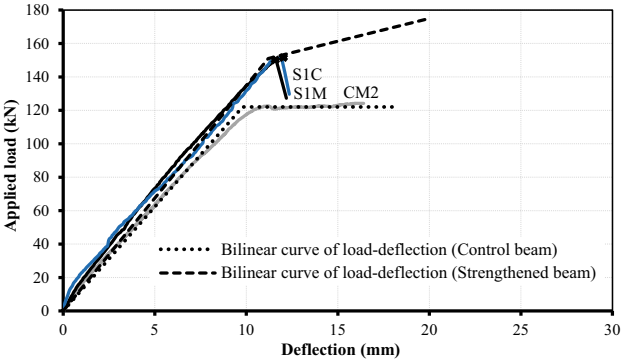

(b) Results of the strengthened beams S1M and S1C

Fig. 10 Experimental results obtained from beam tests.

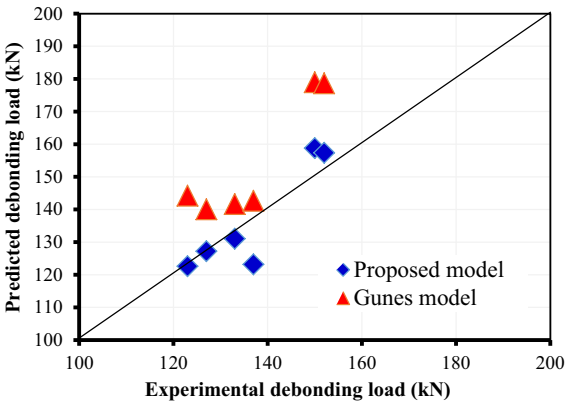

Fig. 11 Comparison of the predictions of proposed model with those of Gunes model.

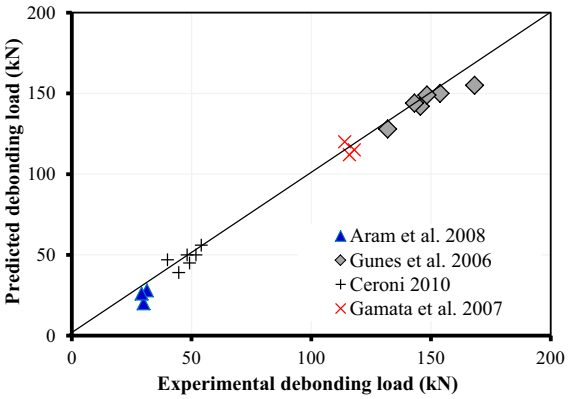

Fig. 12 Model predictions for various sets of experimental data.

predictions of debonding load for the beams of this research which obtained based on Gunes model, along with the predictions of present model were also presented in Fig. 11. As can be found from the figure, Gunes model is less precise than the present one, and gives the predictions much more than the actual values of the test, which seems to be due to the assumptions of the model (stated in earlier sections); while the present model estimates the debonding loads with a good precision. In order to perform further validation of the proposed model, it was tested on a number of experimental data sets produced by various researchers. Implementation of the model to these sets of independently reported data shows that the model can satisfactorily predict the debonding failure loads for various sizes of beams strengthened using FRP reinforcement, with or without bond anchorage (Fig. 12).

5. Conclusions

An analytical model has been developed through experimental study and analytical modeling for predicting the FRP debonding failures. The following conclusions are drawn from the current research.

(1) Experimental results obtained from tested FRP-strengthened beams revealed that providing the end anchorage for the flexural FRP reinforcement plays a significant role in load performance and failure mechanism. Reduction in the load capacity was observed for beams without end anchorage (due to the premature failure through PE debonding of flexural FRP) compared to those with end anchorage. As a result of experimental tests, it is recommended that a minimum bond anchorage is provided at the end regions of the FRP flexural to ensure improved load performance.

(2) While the debonding mode of the strengthened beam that have no end anchorage was PE debonding, that of the remaining strengthened specimens with end anchorages was IC debonding induced by flexural or flexural-shear cracks formed in mid-span or in shear span of the beam.

(3) The proposed analytical model was developed for predicting of the load of debonding failures in RC beams externally strengthened in flexure or flexure/shear by FRP reinforcement.

(4) The model yields a satisfactory prediction of the loads of FRP debonding failure in strengthened beams under both monotonic and cyclic loadings.

(5) The proposed model is able to precisely predict both PE and IC debondings in FRP-strengthened RC beams.

(6) Model was verified by comparing the results with a series of experimental tests carried out by present authors and other researchers. The model shows satisfactory agreement with the experimental results.

(7) A remarkable feature of the model lies in the fact that the effects of the member geometry, strengthening configuration, and bond anchorage is included in the model.

(8) The proposed model does not address cover debonding failures since this failure type appears to be mainly influenced by the shear capacity of the beam. Also, the effect of "bond anchorage" in this model does not include mechanical anchorages such as steel or fiber anchors.

Open Access

References

Achintha, M., & Burgoyne, C. (2011). Fracture mechanics of plate debonding: Validation against experiment. *Construction and Building Materials, 25*, 2961–2971.

Achintha, M., & Burgoyne, C. (2012). Prediction of FRP debonding using the global-energy-balance approach. *Magazine of Concrete Research, 64*(11), 1033–1044.

Achintha, M., & Burgoyne, C. (2013). Fracture energy of the concrete-FRP interface in strengthened beams. *Journal of Engineering Fracture Mechanics, 110*, 38–51.

Bazant, Z. P., & Becq-Giraudon, E. (2001). Statistical prediction of fracture parameters of concrete and implications for choice of testing standard. *Cement and Concrete Research, 32*(4), 529–556.

Bencardino, F., & Condello, A. (2016). Eco-friendly external strengthening system for existing reinforced concrete beams. *Journal of Composites-Part B: Engineering, 93*, 163–173.

Buyukozturk, O., Gunes, O., & Karaca, E. (2002). Characterization and modeling of debonding in RC beams strengthened with FRP composites. In *Proceedings of the 15th ASCE conference on engineering mechanics*. New York, NY: Columbia University.

Ceroni, F. (2010). Experimental performances of RC beams strengthened with FRP materials. *Construction and Building Materials, 24*, 1547–1559.

Ceroni, F., & Pecce, M. (2005). Strength and ductility of RC beams strengthened with FRP materials under monotonic and cyclic loads. The fib symposium on keep concrete attractive, Budapest, Hungary.

Ceroni, F., & Pecce, M. (2010). Evaluation of bond strength in concrete elements externally reinforced with CFRP sheets and anchoring devices. *Journal of Composites for Construction, 14*(5), 521–530.

Ceroni, F., Pecce, M., Matthys, S., & Taerwe, L. (2008). Bond tests on concrete elements with CFRP and anchorage systems. *Journal of Composites-Part B, 39*, 429–441.

Comite Euro-International du Beton-Federation Internationale de la Precontrainte. (1991). CEB–FIP Model Code. Lausanne, Switzerland.

Coronado, C. A., & Lopez, M. M. (2008). Experimental characterization of concrete-epoxy interfaces. *Journal of Materials in Civil Engineering ASCE, 20*(4), 303–312.

Esfahani, M. R., Kianoush, M. R., & Tajari, A. R. (2007). Flexural behavior of reinforced concrete beams strengthened by CFRP sheets. *Engineering Structures, 29*, 2428–2444.

Filiatrault, A., Wanitkorkul, A., & Constantinou, M. (2008). Development and appraisal of a numerical cyclic loading protocol for quantifying building system performance. Report MCEER-08-0013, pp. 3–4.

Galvez, J. C., Elices, M., Guinea, G. V., & Planas, J. (1998). Mixed mode fracture of concrete under proportional and non-proportional loading. *International Journal of Fracture, 94*(3), 267–284.

Gamata, G., Spacone, E., & Zarnic, R. (2007). Experimental and nonlinear finite element studies of RC beams strengthened with FRP plates. *Journal of Composites-Part B: Engineering, 38*, 277–288.

Guinea, G. V., Planas, J., & Elices, M. (1994). A general bilinear fit for the softening curve of concrete. *Materials and Structures, 27*(2), 99–105.

Gunes, O., Karaca, E., & Gunes, B. (2006). Design of FRP retrofitted flexural members against debonding failures. In *Proceedings of the 8th U.S. national conference on earthquake engineering*, San Francisco, CA.

Gustafsson, P. J., & Hillerborg, A. (1985). Improvements in concrete design achieved through the application of fracture mechanics. In S. P. Shah (Ed.), *Application of fracture mechanics to cementitious composites* (pp. 639–680). Dordrecht, Netherlands: Springer, CE.

Hearing B., & Buyukozturk O. (1997). Failure behavior of precracked concrete retrofitted with fiber reinforced plastic laminates. In *Proceedings of the 7th international conference on structural faults and repair*. Edinburgh, UK.

Hutchinson, J. W., & Suo, Z. (1992). Mixed mode cracking in layered materials. *Advances in Applied Mechanics, 191*, 29–63.

Li, V. C., Lim, Y. M., & Foremsky, D. J. (1995). Interfacial fracture toughness of concrete repair materials. In *Proceedings of the 2nd conference on fracture mechanics of concrete structures*. Freiburg, Germany.

Liu, I. S. T., Oehlers, D. J., & Seracino, R. (2007). Study of intermediate crack debonding in adhesively plated beams. *Journal of Composites for Construction, 11*(2), 175–183.

Obaidat, Y., Heyden, S., Dahlblom, O., Abu-Farsakh, G., & Abdel-Jawad, Y. (2011). Retrofitting of reinforced concrete beams using composite laminates. *Construction and Building Materials, 25*(2), 591–597.

Qiao, P., & Xu, Y. (2004). Evaluation of fracture energy of composite–concrete bonded interfaces using three-point bend tests. *Journal of Composite Construction, 8*(4), 352–359.

Reinhardt, H. W. (1985). Crack softening zone in plain concrete under static loading. *Cement and Concrete Research, 15*(1), 42–52.

Saxena, P., Toutanji, H., & Noumowe, A. (2008). Failure analysis of FRP-strengthened RC beams. *Journal of Composites for Construction, 12*(1), 2–14.

Seracino, R., Saifulnaz, M. R. R., & Oehlers, D. J. (2007). Generic debonding resistance of EB and NSM plate-to-concrete joints. *Journal of Composites for Construction, ASCE, 11*(1), 62–70.

Spadea, G., Bencardino, F., Sorrenti, F., & Swamy, R. N. (2015). Structural effectiveness of FRP materials in strengthening RC beams. *Engineering Structures, 99*, 631–641.

Teng, J. G., Chen, J. F., Smith, S. T., & Lam, L. (2002). *FRP strengthened RC structures*. New York, NY: Wiley.

Teng, J. G., Smith, S. T., Yao, J., & Chen, J. F. (2003). Intermediate crack-induced debonding in RC beams and slabs. *Journal of Construction and Building Materials, 17*(6–7), 447–462.

Ulm, F. J., & Coussy, O. (2001). *Mechanics and durability of solids. Solid mechanics* (Vol. I). Prentice Hall series on civil, environmental and systems engineering, Cambridge, MA.

Yao, J., & Teng, J. G. (2007). Plate end debonding in FRP-plated RC beams—I: experiments. *Engineering Structures, 29*, 2457–2471.